DISCRIMINANT ANALYSIS OF OLIVE MILL WASTES USING SPECTRORADIOMETERS IN THE VISIBLE AND NEAR INFRARED PART OF THE SPECTRUM

Athos Agapiou [a,b], Nikos Papadopoulos [b], Apostolos Sarris [b]

[a] Department of Civil Engineering and Geomatics, Faculty of Engineering and Technology, Cyprus University of Technology, 2-6, Saripolou str., 3603, Limassol, Cyprus, athos.agapiou@cut.ac.cy

[b] Laboratory of Geophysical-Satellite Remote Sensing & Archaeo-environment, Institute for Mediterranean Studies, Foundation for Research & Technology, Hellas (F.O.R.T.H.), nikos@ims.forth.gr, asaris@ret.forthnet.gr

Abstract

This paper aims to introduce an Olive Mill Waste index which is able to enhance the detection of olive mill disposal areas using multispectral satellite images. For this purpose several ground spectroradiometric measurements in the range of 450 – 900 nm have been collected at a variety of targets. The samples were initially resampled to the GeoEye-1 sensor using the appropriate Relative Response Filter (RSR) and then scatter plots and spectral signatures were projected. Then an evaluation of nine widely used vegetation indices was performed. This analysis indicated that, Perpendicular Vegetation Index (PVI), Transformed Soil Adjusted Vegetation Index (TSAVI) and Soil and Atmospherically Resistant Vegetation Index (SARVI) are the most efficient to enhance the detection of Olive Mill Waste disposal areas. Moreover, correlation as well as separability analysis have shown than the blue and VNIR spectral bands are the most suitable for interpretation purposes. The Olive Mill Waste index was finally applied to a GeoEye-1 in two cases studies in the island of Crete.

Introduction

Management of olive mill waste water (OMWW) remains a critical and unsolved problem, especially in regions where huge quantities of wastes are produced. Indeed the olive mill wastes (OMW) generated from olive oil extraction is a major environmental issue, particularly in Mediterranean areas [Dermeche et al. 2013]. It is estimated that almost 750 million productive olive trees exists worldwide, while a majority of them (≈98%) being located in the Mediterranean region, where the three major olive oil producers (Spain, Italy, and Greece) worldwide are located [Asfi et al., 2012; Roig, Cayuela and Sánchez-Monedero, 2006]. Therefore olive oil industry is very important in Mediterranean countries, both in terms of wealth and tradition and it is considered to be as one of the driving sectors of the agricultural economy of the Mediterranean basin. OMWW is mainly composed of water (80-83%), organic (15-18%) and inorganic compounds (2%). Although OMWW can be used as natural, low-cost fertilizer, it is actually non-biodegradable and therefore unsuitable for further use as fertilizer or as irrigation water [Niaounakis and Halvadakis, 2006].

In the last years efforts have been made for efficient and ecological management of OOMW disposal areas as well as for the long their term monitoring. In order to avoid environmental impacts, which include soil and air pollution, olive mills were forced to treat or eliminate this OOMW using a variety of techniques and technologies. To this direction current research efforts have been oreinted towards the development of efficient treatment technologies, namely physical, chemical and biological processes as well as various combinations of them [Asfi et al., 2012]. In some Mediterranean countries, untreated OOMW are often discharged directly into sewer systems and water streams or disposed in evaporation ponds/lagoons and soils despite the fact that such management practices are not allowed in most Mediterranean countries [Hanifi and El Hadrami, 2009]. Moreover, no specific European Commission legislation exists today for OMWW management and each country issues different guidelines [Komnitsas et al., 2011].

OMWW disposal areas are generally scattered in different places with diverse loecal topographical and geological settings, while their identification might be difficult and time consuming if it is based purely on in–situ observations. Alternative, satellite remote sensing employing multispectral images seems to be ideal for the detection and systematic monitoring of OOMW disposal areas. As Agapiou et al. [2015] and Alexakis et al [2015] have recently shown, medium and high resolution images can be used to detect OOMW. However difficulties might exist in classification processing as well as detection algorithms due to the spectral similarity of OOMW with other targets. Spectral similarity becomes more difficult in some cases due to the phenomenon of the mixed pixels in the satellite images.

This paper aims to investigate further this spectral similarity as well to identify spectral windows where satellite images can be used so as to enhance the final results. For this purpose spectroradiometric measurements were taken from different targets as descripted in the next section. The spectral signatures were then post-processed through a variety of remote sensing analyses including discriminate analysis; vegetation indices and correlation analysis.

Methodology

In order to accomplish the scientific objectives of this study, laboratory spectroradiometric measurements were taken over the following samples: (a) fresh olive wastes (same day production); (b) dry olive wastes; (c) olive wastes mixed with water (25%); (d) olive wastes mixed with water (50%); (e) olive wastes mixed with soil (25%); (f) olive wastes mixed with water (50%) and soil (50%) and (g) bare soil.

For each one of these samples, 50 spectroradiometric measurements were taken using the GER1500 spectroradiometer. The instrument was set up to collect an average of 5 measurements per sample. GER 1500 spectroradiometer has the ability to record electromagnetic radiation from visible to NIR spectrum (350–1050 nm) using 512 different channels, with a range of ~1.5 nm. Moreover, a lambertian spectralon panel was also used in order to measure the incoming solar radiation and calibrate all the measurements taken over the crops. The field of view (FOV) of the instrument was set to 4 degrees (≈0.02 m^2 from a height

of 1.2 m). At first the incoming radiance was calculated based on the reference measurement at the spectralon panel, while the following measurements were taken over the sample.

Then these narrowband measurements were simulated with the high resolution sensor GeoEye-1 using the appropriate Relative Spectral Response (RSR) filter which was obtained from the operator's website. The spectral band response ρ was simulated by integrating the measured radiances for each target, with the spectral response curve applied as a weighting function, i.e:

$$\rho = \frac{\int_{\lambda 1}^{\lambda 2} w(\lambda) R(\lambda) d\lambda}{\int_{\lambda 1}^{\lambda 2} w(\lambda) I(\lambda) d\lambda} \quad (1)$$

where R is the measured reflected radiation at the top of the canopy as a function of wavelength λ, w is the relative response of the broadband sensor and I is the corresponding incident radiance measured on an ideal reference panel. The actual reference panel measurement I is corrected to the ideal (100% reflectance) by dividing the measured value by its true reflectance $\rho_{ref.}$

$$I(\lambda) = \frac{I\prime(\lambda)}{\rho_{ref}(\lambda)} \quad (2)$$

Based on these broadband reflectance values several vegetation indices as shown in Table 1 were calculated. In detail the Normalized Difference Vegetation Index (NDVI); Simple Ratio (SR); Perpendicular Vegetation Index (PVI); Ratio Vegetation Index (RVI); Transformed Soil Adjusted Vegetation Index (TSAVI); Modified Soil Adjusted Vegetation Index (MSAVI); Soil and Atmospherically Resistant Vegetation Index (SARVI); DVI (Difference Vegetation Index) and Green Normalized Difference Vegetation Index (Green NDVI) were examined. Later, the relative differences between all samples and vegetation indices were calculated.

Table 1. Vegetation indices used for the aims of the study

No	Vegetation Index	Equation	Reference
1	NDVI	$(p_{NIR} - p_{red})/(p_{NIR} + p_{red})$	[Rouse et al., 1974]
2	SR	p_{NIR}/p_{red}	[Jordan, 1969]
3	PVI	$(p_{NIR} - \alpha\, p_{red} - b)/(1+\alpha^2)$	[Richardson and Wiegand, 1977]

		$p_{NIR,soil} = \alpha\ p_{red,soil} + b$	
4	RVI	p_{red}/p_{NIR}	[Pearson and Miller, 1972]
5	TSAVI	$[\alpha(p_{NIR} - \alpha\ p_{NIR} - b)]/[\ (p_{red} + \alpha\ p_{NIR} - \alpha b + 0.08(1+\alpha^2))]$ $p_{NIR,soil} = \alpha\ p_{red,soil} + b$	[Baret and Guyot, 1991]
6	MSAVI	$[2\ p_{NIR}+1-[(2\ p_{NIR}+1)^2-8(p_{NIR} - p_{red})]^{1/2}]/\ 2$	[Qi et al., 1994]
7	SARVI	$(1+0.5)\ (p_{NIR} - p_{rb})/(\ p_{NIR} + p_{rb} + 0.5)$ $p_{rb} = p_{red} - \gamma\ (p_{blue} - p_{red})$	[Kaufman and Tanré, 1992]
8	DVI	$p_{NIR} - p_{red}$	[Tucker, 1979]
9	Green NDVI	$(p_{NIR} - p_{green})/(\ p_{NIR} + p_{green})$	[Gitelson, 1996]

In parallel, the spectral similarity of the samples in the range of 450-900 nm was at first examined through the correlation coefficient (R^2) of all samples in this spectral range. In addition, two main separability indices were evaluated: (a) Euclidean distance and (b) Cosine similarity. Separability indices were performed in order to identify the spectral regions which can be used for the enhancement of the OOMW identification in satellite images.

Results

Spectral Profiles

Scatter plots based on the reflectance values for the GeoEye-1 sensor are shown in Figure 1. As it is observed at the Blue – Green scatter plot, all samples (except soil) tend to give similar reflectance values. Some differences can be recorded in the other three scatter plots (Blue – VNIR; Red-NVIR and Green-VNIR) where the different samples seem to be grouped with a small distance in the 4-D spectral space. However since this spectral distance is quite small (i.e. <5% difference at reflectance values), errors in classification processing are expected due to the spatial resolution and mixed pixels. It should be also noted that soil and the different targets of OOMW examined here tend to give dissimilar reflectance values in all scatter plots. This allows to distinguish these two major group targets (i.e. soil and OOMW) in multispectral images such as the GeoEye-1. The small variations and changes of the "Fresh olive waste (same

day production)" are also noticeable. Small reflectance values are observed for these targets in the blue and green part of the spectrum while the reflectance is increasing in the red and VNIR spectrum. This also indicates that the spectral profile of the OOMW is changing in time in the presence of sun (i.e. dry olive waste), rain (i.e. OOMW with water) or due to the disposal of the environment (i.e. OOMW mixed with soil).

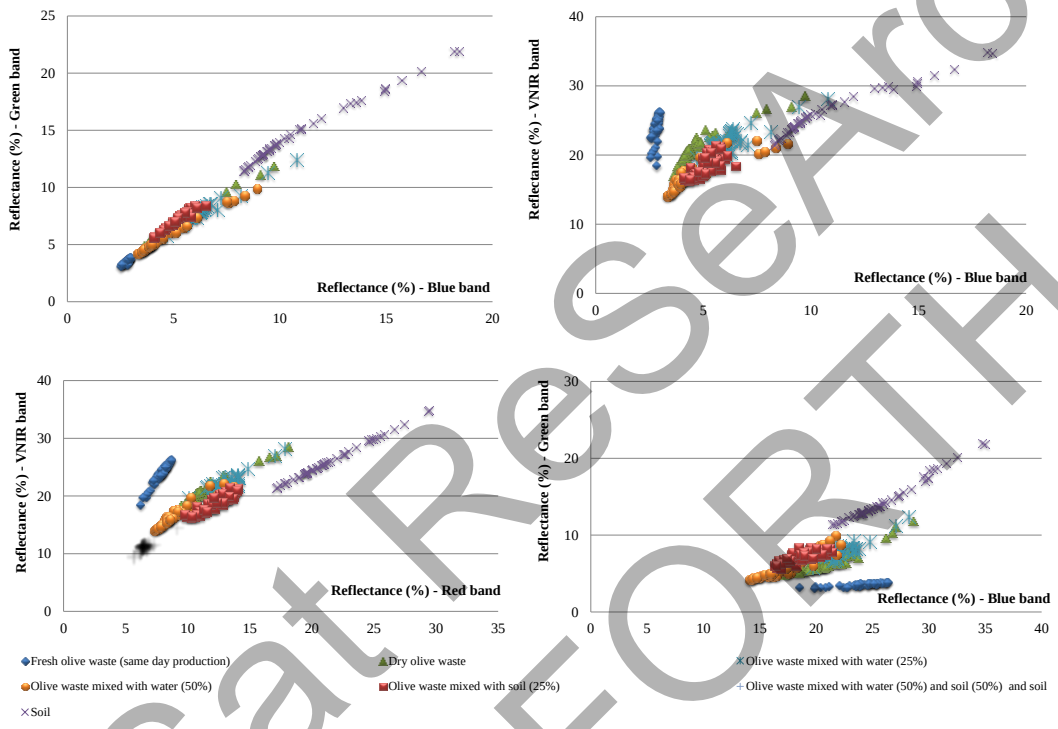

Figure 1: Scatter graph of the Blue-Green band; Blue-VNIR band; Red-VNIR and Blue-Green bands of the samples.

Spectral Profiles

Spectral signatures collected from all samples (fresh olive wastes (same day production); dry olive wastes; olive wastes mixed with water (25%); olive wastes mixed with water (50%); olive wastes mixed with soil (25%); olive wastes mixed with water (50%) and soil (50%) and bare soil) are shown in Figure 2 along with their standard deviations. The dataset was resampled to the GeoEye-1 sensor using equations 1 and 2. As demonstrated in Figure 2, close similarities between the samples do exist, which was also observed from the scatter plots (see Figure 1). These spectral similarities influence classification or detection analysis using satellite images, since the samples may be confused between the different categories. In general in all samples

the lowest reflectance is recorded in the blue band (450-520nm) while higher reflectance values are observed in the VNIR part of the spectrum.

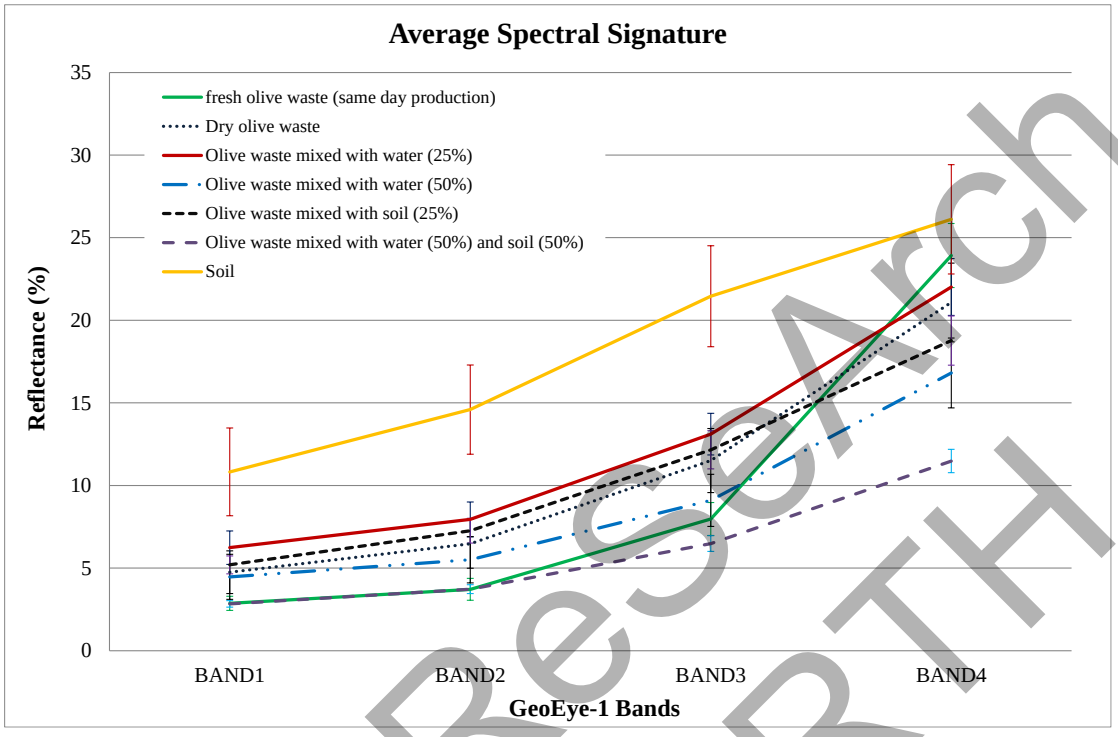

Figure 2: Average spectral signatures as simulated to the GeoEye-1 sensor with their standard deviation.

Vegetation Indices

In an attempt to analyse further the data collected as well as to investigate any potential use of the vegetation indices, well established equations were applied (see Table 1). All spectral signatures were re-calculated to the nine different vegetation indices (based on the GeoEye-1 RSR filter) and their statistics (i.e. mean values) were used for comparison analysis. Relative differences between all samples and all vegetation indices are catalogued in Table 2. Higher relative differences for each sample are also highlighted in the table. As shown some vegetation indices tend to give higher relative difference between the samples. These indices are the PVI, TSAVI and SARVI. Indeed these three vegetation indices tend to give more than 95% of the total higher relative differences compared to the rest of the indices. Although vegetation indices were not designed to distinguish OOMW areas their application in remote sensing images can be useful as demonstrated in this example. SARVI index seems to be quite efficient for the

detection of OOMW areas since it minimizes the atmospheric effects as well the soil background noise in the image.

Table 2. Relative difference (%) between all targets examined in this study. Bold and underlined number indicates the higher relative difference observed in each group of target. Gray values indicate the target which is under investigation. (a) fresh olive wastes (same day production); (b) dry olive wastes; (c) olive wastes mixed with water (25%); (d) olive wastes mixed with water (50%); (e) olive wastes mixed with soil (25%); (f) olive wastes mixed with water (50%) and soil (50%) and (g) bare soil.

Target	NDVI	SR	PVI	RVI	TSAVI	MSAVI	SARVI	DVI	Green NDVI
a									
b	26	24	**35**	24	35	19	8	25	16
c	33	28	43	28	**46**	25	14	28	22
d	25	24	**44**	23	34	19	7	35	18
e	40	32	**60**	32	58	31	39	41	25
f	28	26	61	26	39	22	**62**	52	18
g	67	43	**112**	42	108	58	6	55	44

Target	NDVI	SR	PVI	RVI	TSAVI	MSAVI	SARVI	DVI	Green NDVI
a	26	24	**35**	24	35	19	8	25	16
b									
c	8	5	9	5	**13**	6	6	4	6
d	1	0	10	0	1	0	1	**11**	2
e	16	9	31	9	28	13	**46**	18	9
f	3	2	33	2	5	3	**57**	31	2
g	50	20	**127**	20	117	44	14	35	30

Target	NDVI	SR	PVI	RVI	TSAVI	MSAVI	SARVI	DVI	Green NDVI
a	33	28	43	28	**46**	25	14	28	22
b	8	5	9	5	**13**	6	6	4	6
c									
d	8	5	2	5	**14**	6	7	7	4
e	8	4	23	4	16	7	**50**	15	3
f	5	3	25	3	8	3	**53**	28	4
g	44	16	**134**	16	122	39	20	31	24

Target	NDVI	SR	PVI	RVI	TSAVI	MSAVI	SARVI	DVI	Green NDVI
a	25	24	**44**	23	34	19	7	35	18
b	1	0	10	0	1	0	1	**11**	2
c	8	5	2	5	**14**	6	7	7	4
d									
e	17	9	21	9	29	13	**45**	8	7

f	4	2	24	2	6	3	**58**	21	0
g	50	21	**135**	21	117	44	13	25	28

Target	NDVI	SR	PVI	RVI	TSAVI	MSAVI	SARVI	DVI	Green NDVI
a	40	32	**60**	32	58	31	39	41	25
b	16	9	31	9	28	13	**46**	18	9
c	8	4	23	4	16	7	**50**	15	3
d	17	9	21	9	29	13	**45**	8	7
e									
f	13	7	3	7	23	10	**82**	14	7
g	37	12	**159**	12	133	32	34	17	21

Target	NDVI	SR	PVI	RVI	TSAVI	MSAVI	SARVI	DVI	Green NDVI
a	28	26	61	26	39	22	**62**	52	18
b	3	2	33	2	5	3	**57**	31	2
c	5	3	25	3	8	3	**53**	28	4
d	4	2	24	2	6	3	**58**	21	0
e	13	7	3	7	23	10	**82**	14	7
f									
g	48	18	**163**	18	119	41	66	3	28

Target	NDVI	SR	PVI	RVI	TSAVI	MSAVI	SARVI	DVI	Green NDVI
a	67	43	**112**	42	108	58	6	55	44
b	50	20	**127**	20	117	44	14	35	30
c	44	16	**134**	16	122	39	20	31	24
d	50	21	**135**	21	117	44	13	25	28
e	37	12	**159**	12	133	32	34	17	21
f	48	18	**163**	18	119	41	66	3	28

Correlation analysis

The correlation analysis was based on the narrowband reflectance values of the samples. The Pearson correlation coefficient (R), is used to measure the strength of the linear relationship between two variables (in this case the association between the reflectance in different wavelengths) as shown in equation 3:

$$r = r_{xy} = \frac{\sum_{i=1}^{n}(x_i - \bar{x})(y_i - \overline{y})}{\sqrt{\sum_{i=1}^{n}(x_i - \bar{x})^2}\sqrt{\sum_{i=1}^{n}(y_i - \bar{y})^2}} \quad (3)$$

This investigation will allow to examine which spectral bands (i.e. spectral window) are the optimum for discriminant analysis of the OOMW targets.

Figure 3 indicates the one minus the sample correlation ($1-R^2$) which shows that higher values (indicated with red colour) are observed in the two edges of the spectrum examined in this study (450 nm and 900 nm). These wavelengths correspond to the blue and VNIR bands of the GeoEye-1 sensor. For the rest of wavelengths a strong correlation is visible (< 0.3 in Figure 3). This conclusion is also in line with the results of Figures 1 and 2 where visible bands tend to give similar reflectance values while the VNIR band seems to be more appropriate for detection of OOMW areas in satellite imagery.

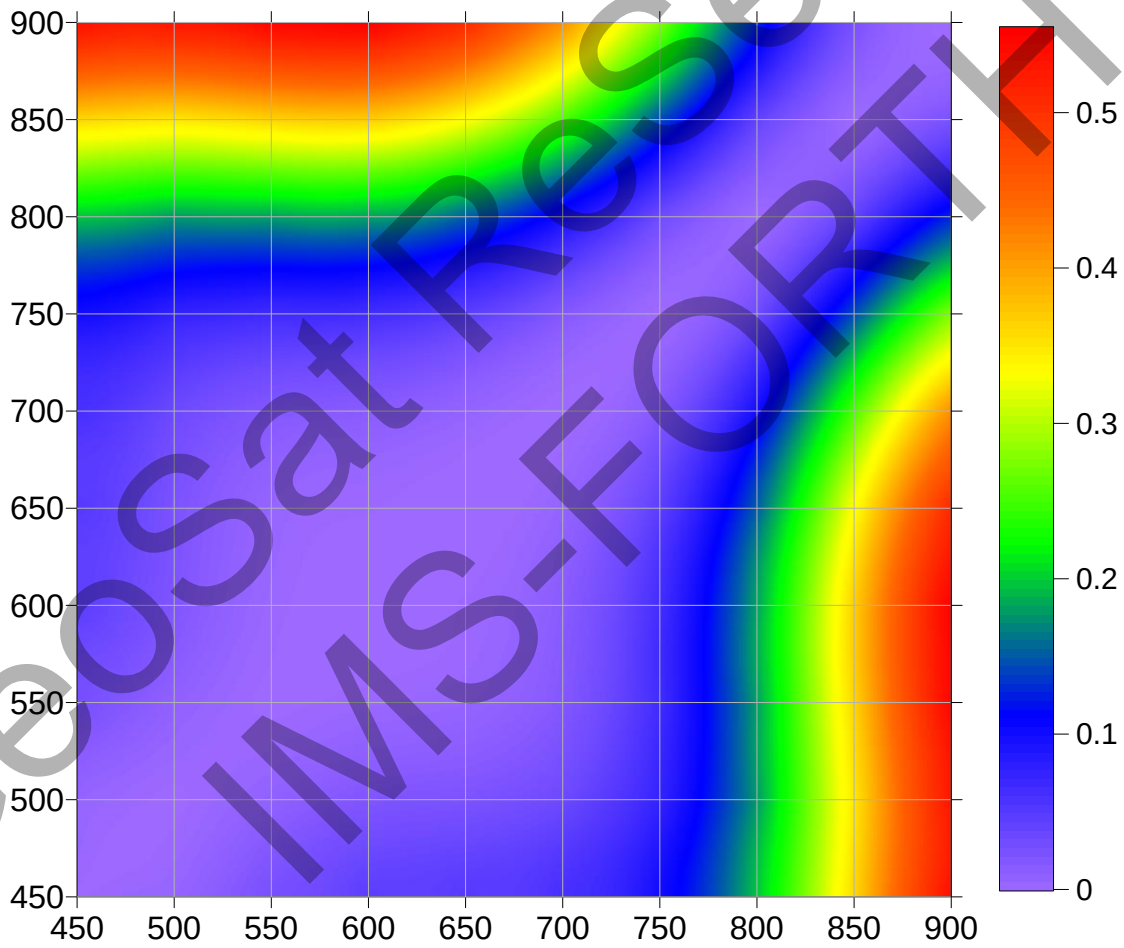

Figure 3: Correlation coefficient results in the range of 450 nm - 900 nm. The figure indicates the one minus the sample correlation.

Separability analysis

Two main algorithms were used to identify spectral regions which are capable to distinguish better the spectral diversity of the different targets examined in this study. These algorithms are

often called separability indices, since they are used to examine the separability of two variables. The purpose of these indicators is to identify whether a group of observations X is separable from another group of observations Y. In this case the Euclidean distance and the Cosine similarity were examined. These algorithms are widely used in classification techniques for satellite images. The Euclidean distance is used in classifications where the minimum distance algorithm is applied, while the Cosine similarity index is exploited to Spectral Angle Mapper (SAM) classification techniques.

(a) Euclidean distance. This method simply calculates the Euclidean distance between a pair of observations. The mathematical equation of Euclidean distance is presented in Equation 4, while the results for both case studies are tabulated in Table 3.

$$d = (px - qx) \quad (4)$$

Where d: Euclidean distance; px and qx are radiations in a specific wavelength.

The final results from the Euclidean distance index are shown in Table 3. Grey values indicate the highest seperability recorded from all dataset.

Table 3. Euclidean distance from all samples in the range of 450 nm-900 nm

	450 nm	**500 nm**	**550 nm**	**600 nm**	**650 nm**	**700 nm**	**750 nm**	**800 nm**	**850 nm**	**900 nm**
450 nm	0									
500 nm	18	0								
550 nm	50	31	0							
600 nm	85	67	35	0						
650 nm	117	99	68	34	0					
700 nm	160	143	113	80	46	0				
750 nm	212	195	167	135	102	56	0			
800 nm	259	243	216	185	153	108	52	0		
850 nm	301	286	260	230	199	154	99	48	0	
900 nm	338	323	298	269	239	194	140	89	41	0

(b) Cosine similarity. The cosine similarity refers to the similarity between two vectors by calculating the cosine of the angle formed by these vectors. The cosine similarity is given by Equation 5. The final results from the Cosine similarity index are shown in Table 4. Grey values indicate the highest seperablity recorded from all dataset.

$$\text{cosine simillarity} = \cos(\varphi) = 1 - (p_x . q_x^T) / ((p_x . p_x T) (q_x . q_x^T)^{0.5} \quad (4)$$

Table 4. Cosine similarity distance from all samples in the range of 450 nm-900 nm

	450 nm	500 nm	550 nm	600 nm	650 nm	700 nm	750 nm	800 nm	850 nm	900 nm
450 nm	0,000									
500 nm	0,001	0,000								
550 nm	0,007	0,002	0,000							
600 nm	0,011	0,005	0,001	0,000						
650 nm	0,014	0,008	0,003	0,001	0,000					
700 nm	0,022	0,016	0,012	0,009	0,003	0,000				
750 nm	0,038	0,033	0,029	0,025	0,015	0,004	0,000			
800 nm	0,057	0,053	0,049	0,045	0,031	0,014	0,003	0,000		
850 nm	0,079	0,075	0,072	0,068	0,051	0,028	0,011	0,003	0,000	
900 nm	0,100	0,096	0,094	0,088	0,069	0,043	0,021	0,008	0,002	0,000

The final results from both separability indices indicate that the spectral regions of 450nm and 900 nm are the most optimal for detection of OOMW targets. Therefore using these spectral regions (i.e. Blue and VNIR in the GeoEye-1 image) OOMW areas should be enhanced better than any other spectral combination.

Discussion

Separability analysis identified that the blue and VNIR part of the spectrum are the optimum two wavelength regions for the detection of OOMW. This is also indicated and confirmed by the correlation analysis (see Figure 3). Indeed correlation analysis shows that these two spectral regions at around 450 nm and 900 nm tend to be the most un-correlated. In a similar way the results from the scatter plots and the spectral signatures of the target (see Figure 1 and Figure 2 respectively) indicate that the maximum spectral distance is observed in the Blue and VNIR bands of the GoeEye-1 sensor.

These observations are also in agreement with the outcomes from the vegetation indices analysis. As it was found, the most promising indices were the PVI, TSAVI and SARVI. The calculation for these specific three indices is based on the blue band. Although the blue band is mainly used as a “correction” coefficient to these indices (i.e. removal of atmospheric effects in the satellite images), its use gives the highest relative difference among all the broadband vegetation indices examined here.

The overall results from this study were applied using a GeoEye-1 pan sharpen image taken over the island of Crete in June 16th 2013. As it is indicated in Figure 4 (left) some OOMW disposal areas can be spotted using interpretation of the image. Figure 4 (right) is the same area after the application of the normalized OOMW index (shown in equation 5) as found from the discriminant analysis in the previous sections. The results show that OOMW disposal areas can be enhanced after the application of the proposed index.

$$\text{Normalized Index}_{OOMW} = (\rho_{VNIR} - \rho_{Blue}) / (\rho_{VNIR} + \rho_{Blue}) \quad (5)$$

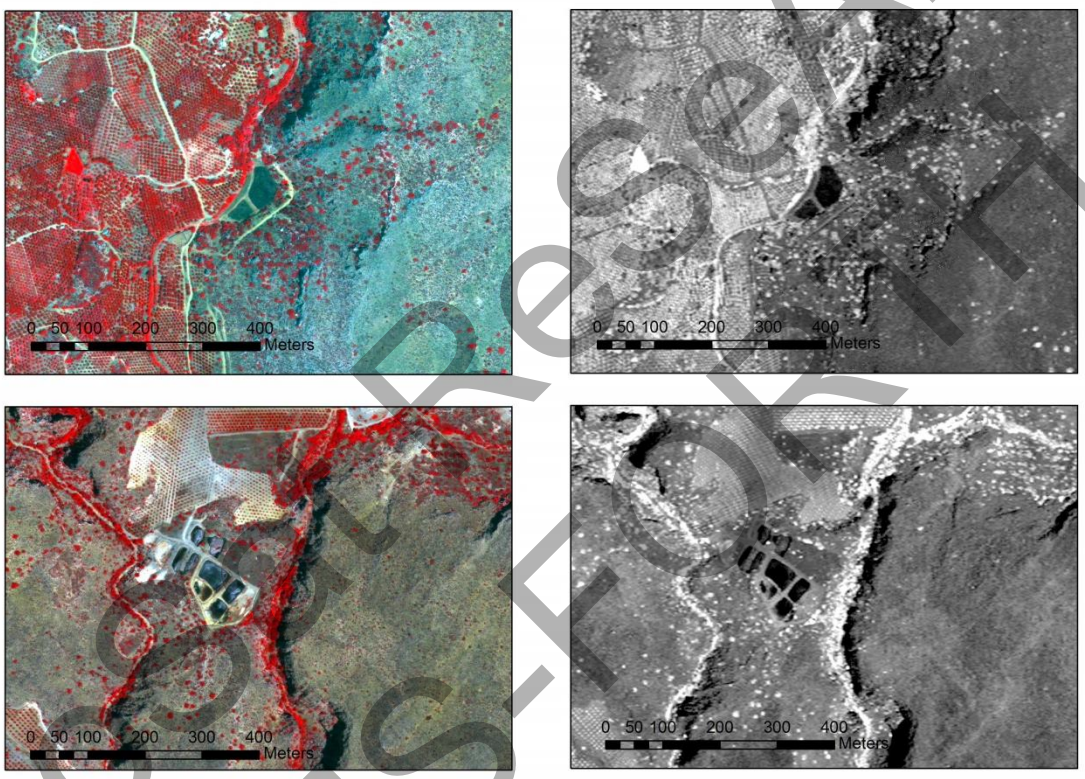

Figure 4: Two examples from OOMW disposal areas in Crete as seen in the GeoEye-1 image (left) in the VNIR-R-G pseudo color composite. In the right the same area after the application of the normalized VNIR – Blue band. The OMW disposal areas are highlighted as dark objects in the scene.

Conclusions

Olive production industry is of great importance for Mediterranean countries. Therefore a sustainable management of the whole cycle of olive production needs to be taken into consideration so as to minimize and eliminate the environmental problems related with the OOMW disposal areas.

This paper aims to highlight the contribution of satellite remote sensing as a tool for systematic and effective way for monitoring OMWW disposal areas. As previous studies have shown [Agapiou et al., 2015; Alexakis et al. 2015] remote sensing can be used for detection of OMWW areas.

In order to achieve better results in satellite images, this paper has investigated several samples related with OOMW using ground spectroradiometers. Discriminant analysis was carried out in the samples collected and the final results have shown that the spectral region in the 450 nm and 900 nm can be used so as to detect better OOMW disposal areas. This conclusion was observed in a variety of remote sensing analysis: from simple scatter plots and spectral signatures, to vegetation indices as well to separability indices.

The proposed normalised OOMW index was applied to a GeoEye-1 multispectral image successfully, improving the interpretation of the image. The overall results suggest that satellite remote sensing images can be used sufficiently for detecting and monitoring OOMW disposal areas in the whole life cycle (from fresh olive waste to mixed olive waste with soil).

Acknowledgments

This work was performed in the framework of the PEFYKA project within the KRIPIS Action of the GSRT. The project is funded by Greece and the European Regional Development Fund of the European Union under the NSRF and the O.P. Competitiveness and Entrepreneurship.

References

Agapiou, A., Papadopoulos N., Sarris A., 2015. Detection of olive oil mill waste (OOMW) disposal areas in the island of Crete using freely distributed high resolution GeoEye's OrbView-3 and Google Earth images, Remote Sensing Letters, (submitted)

Alexakis, D.D.., Sarris, A., Kalaitzidis, C., Papadopoulos, N., Soupios, P., 2015. Integrated use of satellite remote sensing, GIS and ground spectroscopy techniques for monitoring olive oil mill waste disposal areas in Crete Island –Greece. International Journal of Remote sensing, (accepted for publication in International Journal of Remote Sensing).

Asfi, M., Ouzounidou, G., Panajiotidis, S., TherioS, I., Moustakas, M., 2012. Toxicity effects of olive-mill wastewater on growth, photosynthesis and pollen morphology of spinach plants. Ecotoxicology and Environmental Safety, 80(1), 69-75,

Baret, F.; Guyot, G. Potentials and limits of vegetation indices for LAI and APAR assessment. Remote Sens. Environ. 1991, 35, 161–173.

S. Dermeche, M. Nadour, C. Larroche, F. Moulti-Mati, P. Michaud, 2013. Olive mill wastes: Biochemical characterizations and valorization strategies, Process Biochemistry, Volume 48, Issue 10, October 2013, Pages 1532-1552, ISSN 1359-5113, http://dx.doi.org/10.1016/j.procbio.2013.07.010.

Gitelson, A. A.; Kaufman, Y. J.; Merzlyak, M. N. Use of a green channel in remote sensing of global vegetation from EOS-MODIS. Remote Sens. Environ. 1996, 58, 289–298.

Hanifi, S., El Hadrami, I. 2009. Olive mill wastewaters: Diversity of the fatal product in olive oil industry and its valorisation as agronomical amendment of poor soils. A review. Journal of Agronomy, 8,1–13.

Jordan, C.F. Derivation of leaf area index from quality of light on the forest floor. Ecology 1969, 50, 663–666.

Kavvadias, V., Doula, M., TheocharopouloS, S., 2014. Long-Term Effects on Soil of the Disposal of Olive Mill Waste Waters (OMW). Environmental Forensics, 15(1), 37-51.

Kaufman, Y.J.; Tanré, D. Atmospherically resistant vegetation index (ARVI) for EOS-MODIS. IEEE Trans. Geosci. Remote Sens. 1992, 30, 261–270.

Komnitsas, K., Zaharaki, D., Doula, M., Kavvadias, V., 2011. Origin of recalcitrant heavy metals present in olive mill wastewater evaporation ponds and nearby agricultural Soils. Environmental Forensics, 12, 319–326.

Niaounakis, M., Halvadakis, C. P., 2006. Olive processing waste management. Literature review and patent survey. Waste Management Series, 5, Elsevier Ltd.

Pearson, R.L.; Miller, L.D. Remote Mapping of Standing Crop Biomass and Estimation of the Productivity of the Short Grass Prairie, Pawnee National Grasslands, Colorado. In Proceedings

of the 8th International Symposium on Remote Sensing of the Environment, Ann Arbor, MI, USA, 2–6 October 1972; pp. 1357–1381.

Qi, J.; Chehbouni, A.; Huete, A.R.; Kerr, Y.H.; Sorooshian, S. A modified soil adjusted vegetation index. Remote Sens. Environ. 1994, 48, 119–126.

Richardson, A.J.; Wiegand, C.L. Distinguishing vegetation from soil background information. Photogram. Eng. Remote Sensing. 1977, 43, 15–41.

Roig, A., Cayuela, M.L., SáncheZ-monedero, M.A., 2006. An overview on olive mill wastes and their valorisation methods. Waste Management, 26(9), 960-969.

Rouse, J.W.; Haas, R.H.; Schell, J.A.; Deering, D.W.; Harlan, J.C. Monitoring the Vernal Advancements and Retrogradation (Greenwave Effect) of Nature Vegetation; NASA/GSFC Final Report; NASA: Greenbelt, MD, USA, 1974.

Tucker, C.J. Red and photographic infrared linear combinations for monitoring vegetation. Remote Sens. Environ. 1979, 8, 127–150.